Granular Matter (2019) 21:92
https://doi.org/10.1007/s10035-019-0944-0

ORIGINAL PAPER

Acoustic emission generated by glass beads in compression and shearing

Alister Smith[1] · **Neil Dixon**[1]

Received: 8 April 2019

Abstract
Acoustic emission (AE) monitoring offers the potential to sense particle-scale interactions that lead to macro-scale responses of granular materials. This paper presents results from a programme of drained triaxial tests performed on densely packed glass beads to establish quantitative interpretation of AE during isotropic compression, shearing and associated stick–slip events. Relationships have been quantified between: AE and boundary work (i.e. AE generated per Joule) for a unit volume of glass beads under isotropic compression and shear; AE and shear displacement rate; and the amplitude of deviator stress cycles and AE activity during stick–slip events. In shear, AE generation increased with shear strain and reached peak values that were maintained from volume minimum (i.e. the transition from contractive to dilative behaviour) to peak dilatancy, whereupon AE generation gradually reduced and then remained around a constant mean value with further increments of shear strain. In each stick–slip event, AE activity increased during shear strength mobilisation, particle climbing and dilation, and then reduced with the subsequent deviator stress drop during particle sliding and contraction. The amplitude of these cycles in AE activity were governed by the amplitude of deviator stress cycles during stick–slip events, which were also proportional to the imposed stress level and inversely proportional to particle size.

Keywords Acoustic emission · Deformation · Friction · Granular media · Monitoring · Stick–slip

List of symbols

A	AE waveform amplitude
B	Skempton's pore pressure parameter
b-value	Measure of the proportion of low and high magnitude events in an AE waveform
C_c	Coefficient of curvature
C_u	Coefficient of uniformity
D_r	Relative density (%)
d_{50}	Mean particle size
e_{max}	Maximum void ratio
e_{min}	Minimum void ratio
M	Frictional constant defining the slope of the critical state line in q–p′ space ($6\sin\phi'_{cv}/3-\sin\phi'_{cv}$)
m	Log-scale measure of AE magnitude
p'	Mean effective stress (kPa)
q	Deviator stress (kPa)
R_a	Roughness average: the arithmetic average of the absolute values of the profile heights over the evaluation length (μm)
R_q	RMS Roughness: the root mean square average of the profile heights over the evaluation length (μm)
R_z	Average maximum height of the profile: the average of the successive values of the vertical distance between the highest and lowest points of the profile within a sampling length calculated over the evaluation length (μm)
RDC	Ring-down counts are the number of times the AE waveform crosses a voltage threshold level
ΔW	Increment of work done per unit volume transmitted to the granular material across its boundaries (i.e. boundary work)
ΔW_d	Increment of distortional work per unit volume
ΔW_v	Increment of volumetric work per unit volume
ε_a	Axial strain
ε_r	Radial strain
ε_{vol}	Volumetric strain
ε_γ	Shear strain $\left(\varepsilon_a-\varepsilon_r=\frac{1}{2}\left(3\varepsilon_a-\varepsilon_{vol}\right)\right)$

✉ Alister Smith
A.Smith10@lboro.ac.uk

[1] School of Architecture, Building and Civil Engineering, Loughborough University, Loughborough, UK

Published online: 27 August 2019

ε_q	Deviatoric strain $\left(\frac{2}{3}\varepsilon_\gamma = \frac{2}{3}(\varepsilon_a - \varepsilon_r) = \varepsilon_a - \frac{1}{3}\varepsilon_{vol}\right)$
$\rho_{dry}max$	Maximum dry density $\left(Mg/m^3\right)$
$\rho_{dry}min$	Minimum dry density $\left(Mg/m^3\right)$
ρ_s	Particle density $\left(Mg/m^3\right)$
σ'_r	Radial effective stress (kPa)
ϕ'_{cv}	Constant volume friction angle
ϕ'_p	Peak effective friction angle

1 Introduction

Proportions of the energy dissipated during deformation of particulate materials are converted to heat and sound. The high-frequency (> 10 kHz) component of this sound energy is called acoustic emission (AE). The AE behaviour of particulate systems has been studied in the context of a range of disciplines, including: soil mechanics (e.g. [1–4]), landslides (e.g. [5–8]), faulting and earthquakes (e.g. [9, 10]), granular physics (e.g. [11–13]), additive manufacturing (e.g. [14]), mining (e.g. [15]) and pharmaceuticals (e.g. [16, 17]).

Densely packed particulate materials mobilise shearing resistance through inter-particle friction and interlocking (i.e. dilation, particle rearrangement and particle damage) [18]. AE monitoring offers the potential to sense particle-scale interactions that lead to macro-scale responses of granular materials, for example: particle–particle interactions such as sliding and rolling friction; particle contact network rearrangement (e.g. release of contact stress and stress redistribution as interlock is overcome and regained); degradation at particle asperities; and crushing [4, 5, 19]. Monitoring the evolution of these processes is particularly valuable in geotechnical engineering, where mobilisation of peak shear strength in dense soils causes shear zones to develop, which in turn leads to reduced shear strength and accelerating deformation behaviour as the soil mass becomes weaker under the same imposed boundary stresses; this ultimate limit state can have devastating consequences for people and infrastructure.

Smith and Dixon [4] demonstrated the benefits of using AE to monitor the behaviour of dense sands in triaxial experiments, and they proposed a framework to interpret the mobilisation of peak shear strength and to quantify rates of shear strain from AE measurements. The study also demonstrated the influences of the fabric (i.e. orientation and distribution of particle contacts) and state (i.e. physical condition, including stresses and void ratio) of sands on AE generation. However, stick–slip behaviour was not investigated because the natural quartz Leighton Buzzard sand that was studied exhibited negligible stick–slip events.

Glass beads are often used in the investigations of granular media behaviour (e.g. [10, 12, 19–21]) because of their relatively uniform and well understood properties. However, to date, interpretation of AE generated by glass beads has been qualitative (e.g. higher AE activity indicating a more significant stick–slip event [12]) and studies have not developed a quantitative framework for interpretation of material behaviour. The objective of the research reported here was to holistically develop quantitative interpretation of the AE behaviour of densely packed glass beads encompassing isotropic compression, shearing and associated stick–slip events. To achieve this, a programme of drained triaxial isotropic compression and shearing experiments were performed on samples of glass beads and AE measurements were compared with mechanical behaviours (e.g. stresses, strains and boundary work). The new quantitative methods will enable the evolution of particulate material behaviour to be interpreted from AE measurements, potentially removing or reducing the need for arduous measurements of stresses and strains, and hence benefitting a wide range of applications and industries.

2 Methodology

2.1 Apparatus

Triaxial tests enabled the systematic investigation of the evolution of AE with the stress–strain response of glass beads at a range of effective confining stresses and strain rates under drained conditions. The advantages of triaxial testing over simpler procedures, such as direct-shear testing, include the ability to control specimen drainage and stress conditions. A hydraulic GDS Bishop and Wesley [22] stress path triaxial apparatus was used to eliminate noise that could be generated by motor-operated systems. A schematic of the apparatus is shown in Fig. 1, which has a bespoke 50 mm diameter base pedestal incorporating both AE and pore-water pressure measurement.

2.2 Glass beads

Glass beads were selected for this investigation as their mechanical behaviour has been studied extensively in the literature (e.g. [9, 19, 21]) and batches of different size fractions could be procured with consistent properties. Four poorly-graded, single-sized glass bead materials were selected to promote stick–slip behaviour during shearing, minimise the influence of different fabrics and to control mineralogy, shape, surface roughness and inter-particle friction.

The physical properties of the glass beads are shown in Table 1 and their particle size distributions are shown in Fig. 2. The mean particle sizes (i.e. d_{50}) were 2.67 mm (GB 4510), 1.61 mm (GB 4506), 0.81 mm (GB 4503) and 0.52 mm (GB 45015). Particle size and packing properties

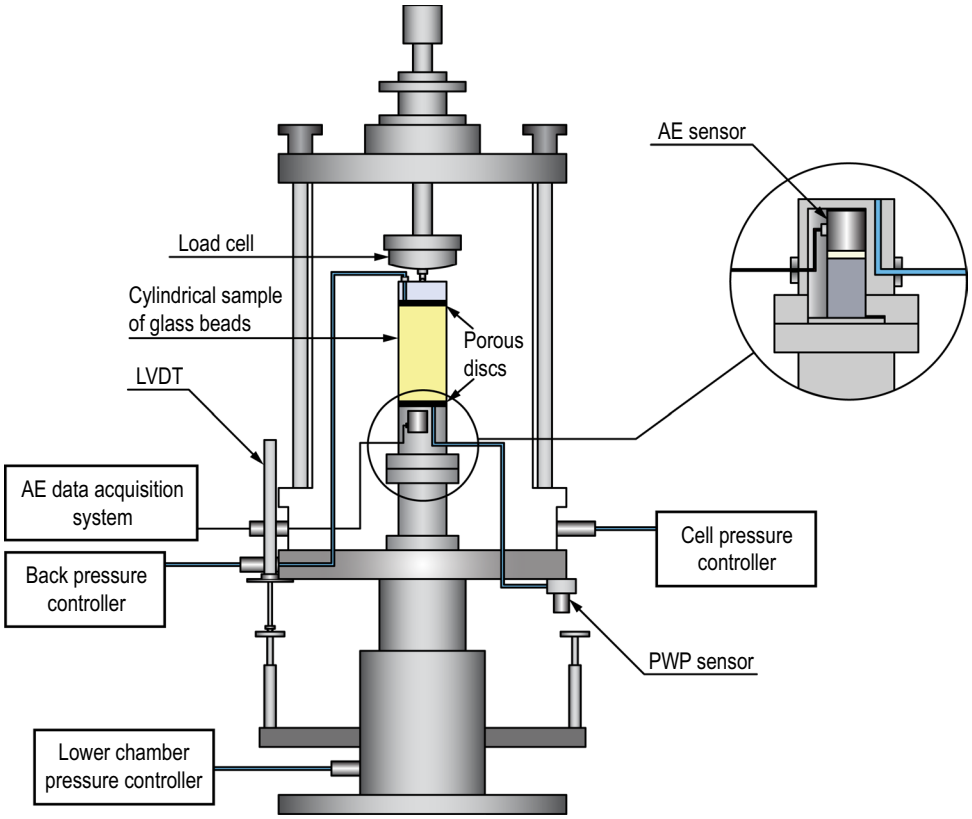

Fig. 1 Schematic of the GDS Bishop and Wesley Stress Path triaxial apparatus and modified base pedestal to incorporate both AE and pore-water pressure measurement (after Smith and Dixon [4])

were quantified using soils testing methods to BSI [23]. Particle shape parameters (range and mean) were quantified from measurements of 40 particles taken across the four particle size ranges. Roundness and sphericity were computed using the method described in Zheng and Hryciw [24] from 2D microscope images of the particles. Roundness is quantified as the average radius of curvature of particle surface features relative to the radius of the largest circle that can be inscribed in the particle. Sphericity (circle ratio) is quantified as the diameter ratio between the largest inscribing and smallest circumscribing circles [24–27]. The range of roundness measurements was 0.92 to 1.00 and the mean was 0.99. The range of sphericity measurements was 0.90 to 0.99 and the mean was 0.97. Roughness was computed using high-resolution optical 3D measurements of the particles acquired with an Alicona Infinite Focus system. Roughness parameters R_a, R_q and R_z are the roughness average, RMS roughness and average maximum profile height, respectively. The range of R_a (μm) measurements was 0.16 to 1.23 and the mean was 0.57. The range of R_q (μm) measurements was 0.21 to 1.64 and the mean was 0.78. The range of R_z (μm) measurements was 0.56 to 5.09 and the mean was 2.39. Scanning electron microscope (SEM) images of a glass bead particle are shown in Fig. 3.

2.3 Testing procedure

Specimen preparation followed the same procedure to that described in Smith and Dixon [4] for sand samples. The cylindrical specimens were 50 mm in diameter and 100 mm tall. Samples were prepared in a membrane-lined split-mould mounted on the base pedestal. Moist compacted samples were tamped into the mould to a target relative density, D_r, of approximately 85% in 10 equal layers to produce densely packed assemblages of glass beads. Back pressure of 400 kPa was imposed under a constant effective stress of approximately 20 kPa to achieve saturation until a minimum pore-pressure parameter, B, of 0.97 was measured [18, 28–30].

Isotropic compression was performed by increasing the cell pressure to achieve a target effective stress (e.g. 100, 200 or 300 kPa), which led to excess pore-water pressure generation and consolidation. The drainage pathway was through the upper porous disc and top cap (Fig. 1) and the volume of water leaving the samples was measured by the back-pressure controller. Pore-water pressure measurement was at the base of the specimens.

The shearing stage was initiated after no further volume change took place and 100% of the excess pore-water pressure had dissipated. Shearing was performed strain-controlled through application of constant rates of axial displacement of 1, 3 and 6 mm/h, which were selected to

Table 1 Physical properties of the glass beads

Description		Particle size			Packing				
		Size range (mm)	C_u	C_c	ρ_s	ρ_{dry}min	ρ_{drymax}	e_{min}	e_{max}
Glass Beads	GB 4510	2.40–2.90	1.318	0.954	2.500	1.510	1.531	0.633	0.656
	GB 4506	1.55–1.85	1.325	0.985		1.530	1.558	0.605	0.634
	GB 4503	0.75–1.00	1.431	0.931		1.550	1.572	0.590	0.613
	GB 45015	0.40–0.60	1.410	0.944		1.550	1.584	0.578	0.613

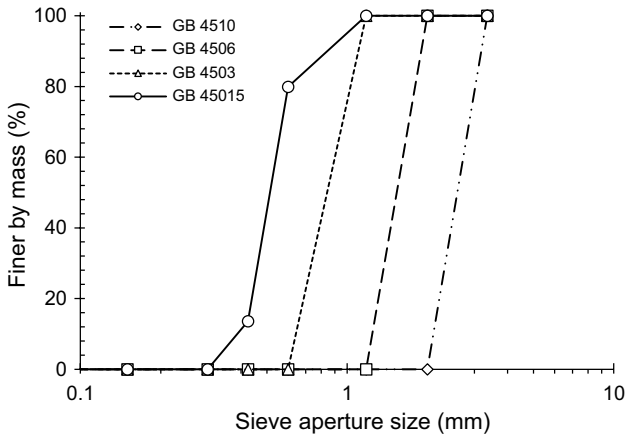

Fig. 2 Particle size distributions of the glass beads

ensure drained shearing. The appropriate corrections for the membrane and changes in specimen area were applied to the measurements [28].

A summary of the triaxial tests performed in this investigation is shown in Table 2. The peak and critical state friction angles obtained are typical and consistent with those reported for glass beads in the literature (e.g. [9, 21, 31]).

2.4 Energy calculations

Equations 1–3 were used to quantify the work done during the triaxial experiments for comparison with AE measurements. The increment of work done per unit volume transmitted to the granular material across its boundaries (i.e. boundary work) was computed using Eq. 1. Boundary work per unit volume has two components: distortional work per unit volume, which causes a change of sample shape (Eq. 2); and volumetric work per unit volume, which causes a change of sample volume (Eq. 3) [32–35].

$$\Delta W = \Delta W_d + \Delta W_v \tag{1}$$

$$\Delta W_d = q\delta\varepsilon_q = \frac{2}{3}q\delta\varepsilon_\gamma \tag{2}$$

$$\Delta W_v = p'\delta\varepsilon_{vol} \tag{3}$$

where $\delta\varepsilon_\gamma$, $\delta\varepsilon_q$ and $\delta\varepsilon_{vol}$ are increments of shear strain, deviatoric strain and volumetric strain, respectively. The increments of work done per unit volume were multiplied by the current sample volume in each increment [35]. This allowed direct comparison with the AE generated by each sample, and hence the AE generated for an increment of work done per unit volume.

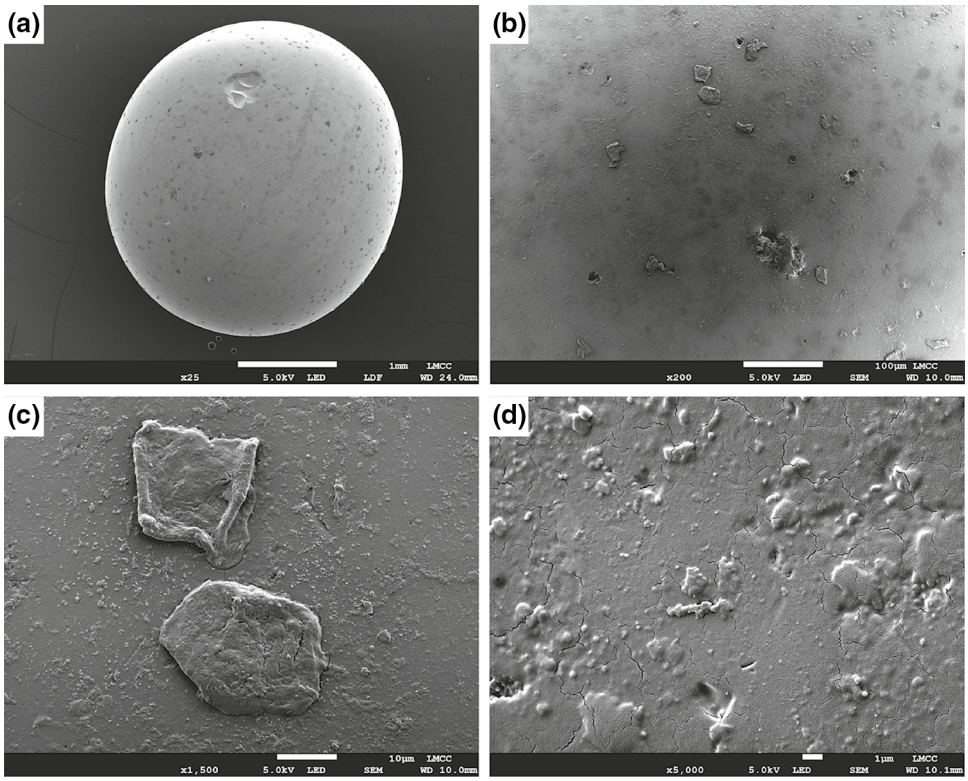

Fig. 3 Scanning electron microscope (SEM) images of a glass bead particle. The length of the white bar in the bottom panel of each image shows the scale: 1 mm in (**a**), 100 µm in (**b**), 10 µm in (**c**), and 1 µm in (**d**). Note that cracking visible in (**d**) is in the gold–palladium sputter coating on the surface of the particle, which is required for SEM imagery

Table 2 Summary of the drained triaxial isotropic compression and shearing tests performed in this study

Test No.	Material	σ'_r (kPa)	Axial displacement rate (mm/h)	Initial D_r (%)	ϕ'^{b}_p	ϕ'^{b}_{cv}	M^b
1	GB 45015	100	1	84.4	31°	23°	0.89
2	GB 45015	200	1	84.4			
3	GB 45015	300	1	84.4			
4	GB 4503	100	1	83.7	31°	23°	0.89
5	GB 4503	200	1	83.7			
6	GB 4503	300	1	83.7			
7	GB 4506	100	1	84.8	31°	23°	0.89
8	GB 4506	200	1	84.8			
9	GB 4506	300	1	84.8			
10	GB 4506	300	3	84.8			
11	GB 4506	300	6	84.8			
12	GB 4510	100	1	85.9	31°	23°	0.89
13	GB 4510	200	1	85.9			
14	GB 4510	300	1	85.9			
15[a]	GB 4506	–	–	84.8	–		

[a]Isotropic load–unload–reload (LUR) cycles of σ'_r

[b]Friction parameters obtained from drained triaxial shearing tests performed in this study at three different cell pressures

2.5 Acoustic emission measurements

A band-pass filter was used to constrain the measured AE to within the frequency range of 10–100 kHz. Filtering signals below 10 kHz is essential to remove extraneous low-frequency environmental noise that could be generated in a laboratory by machinery. The focus of this investigation was frictional and stick–slip interactions within assemblages of glass beads; particle damage and fracturing were minimised through application of relatively low effective

confining stress (100–300 kPa). Mao and Towhata [36] found that particle crushing has a much higher frequency content (> 100 kHz) than inter-particle friction and particle rearrangement (< 100 kHz). It is notable that particle damage was minimal in the experiments reported here (confirmed through post-test particle size distributions), and hence filtering above 100 kHz was appropriate for this study.

The AE sensor was installed inside the base pedestal as shown in Fig. 1; a 5 mm wall of stainless steel separated the surface of the sensor and the top surface of the pedestal. The sensor was a MISTRAS R3α piezoelectric transducer, which is sensitive over the frequency range of 0–100 kHz and has a resonant frequency of 30 kHz. The sensor converts the mechanical AE to a voltage waveform that can be processed.

The AE measurement system was a bespoke setup comprising a pre-amplifier (20 dB gain), a main amplifier (3 dB gain), an analogue-to-digital converter with 2 MHz sampling frequency, and a laptop with a LabView program to condition, process and record the AE waveform. The two amplifiers were used to improve the signal-to-noise ratio. The LabView program was set to further attenuate signals outside of the 10–100 kHz range and record the full AE waveform within this frequency range.

Two key AE parameters of interest are ring-down counts (RDC) and *b-value*. RDC per unit time are the number of times the AE waveform crosses a programmable threshold level (set to 0.01 V in this study, above background environmental and electronic noise as shown in Fig. 4) within a predefined time interval and are a measure of the AE signal energy. The *b-value* can be obtained from the full AE waveform data [37] and is a convenient way to describe the amplitude distribution in a single value. When the AE waveform is dominated by low amplitude events the *b-value* is large. As the proportion of higher amplitude events increases, indicating an increase in energy, the *b-value* reduces. The *b-value* was computed at 1-min intervals using Eqs. 5 and 6.

$$\log N = c - bm \tag{5}$$

$$m = \log A \tag{6}$$

where A is the amplitude, m is a log-scale measure termed magnitude, N is the number of AE events with magnitude greater than m, c is the point that the *log(N)* vs. *m* relationship intersects the y-axis, and the coefficient b (*b-value*) is the negative slope of the *log(N)* vs. *m* relationship.

Quantifying the *b-value* is appropriate as the measured *log(N)* vs. *m* relationships follow a power law, as demonstrated through multiple studies reported in the literature on AE monitoring of particulate materials (e.g. [3, 4, 12, 19, 20]).

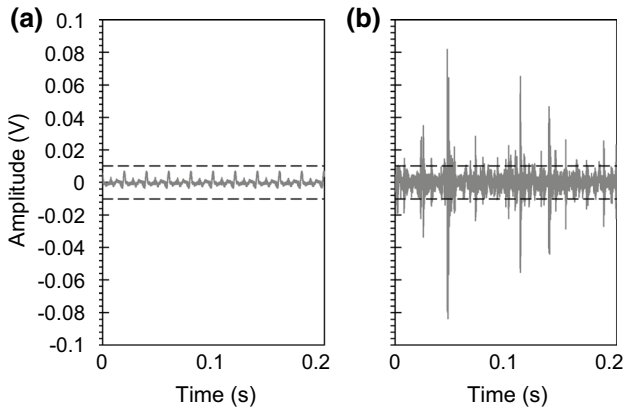

Fig. 4 Example waveforms recorded using the AE measurement system showing the 0.01 V threshold level: **a** background environmental and electronic noise, and **b** during deformation of granular media (after Smith and Dixon [4])

3 Results

3.1 Isotropic compression

Figure 5 shows example time series measurements from isotropic compression performed on GB 4503 (d_{50} = 0.81 mm) (Tests 4, 5 and 6). Space precludes inclusion of time series measurements from all tests; however, the general trends in behaviour were the same, and results from all isotropic compression tests (Tests 1–9 and 12–14) are compared in relation to the change in mean effective stress and volumetric work done in Fig. 6. Excess pore-water pressures developed as the imposed cell pressure increased in each test. With time the mean effective stress increased as the excess pore-water pressure dissipated, and the specimen consolidated to a drained condition.

The small increase in volume shown at 4 min and decrease at 7.5 min in the measurements for cell pressure to 300 kPa in Fig. 5c (i.e. solid black line) are a function of the measurement system. During tests, the volume of de-aired water in the back-pressure controller is automatically modified at regular intervals in order to maintain a constant back-pressure in response to changes in cell pressure. Note that the *b-value* measurements were not significantly modified by isotropic compression; however, they were influenced by stick–slip behaviour in shear (described later).

Figure 6a shows the total AE generated during isotropic compression increased proportionally with the change in mean effective stress; however, these data also show that AE generation was influenced by particle size. Figure 6b shows the total AE generated plotted against the volumetric work done, which results in stronger correlation (e.g. R^2 values of 0.92 and 0.96 for the presented linear and exponential relationships, respectively). The linear regression in Fig. 6b, which excludes the data corresponding to volumetric work

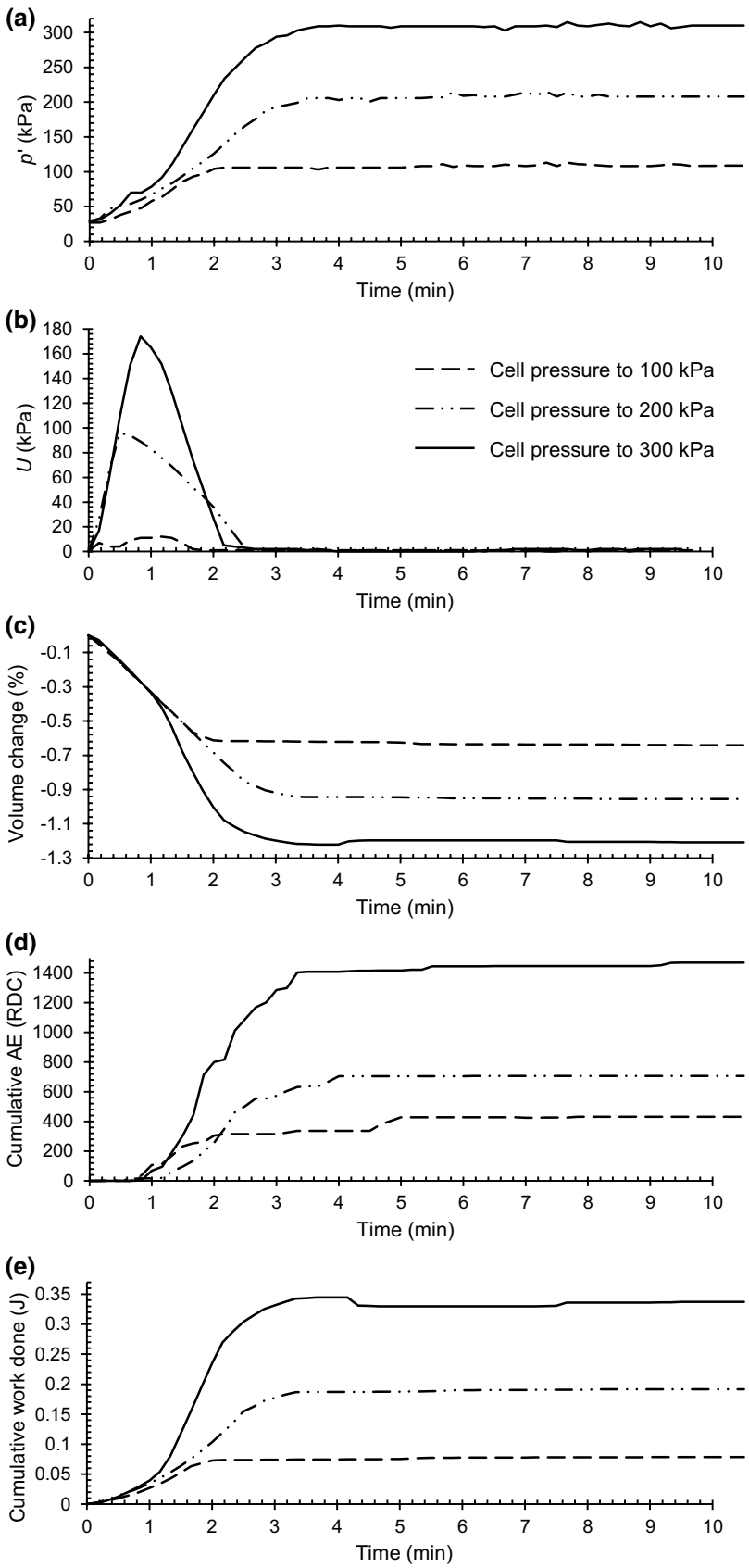

Fig. 5 Time series measurements from isotropic compression tests to effective confining pressures of 100, 200 and 300 kPa performed on GB 4503 (d_{50} = 0.81 mm) (Tests 4, 5 and 6). **a** mean effective stress, **b** excess pore-water pressure, **c** volume change (%), **d** cumulative AE (RDC), and **e** cumulative volumetric work (Joules)

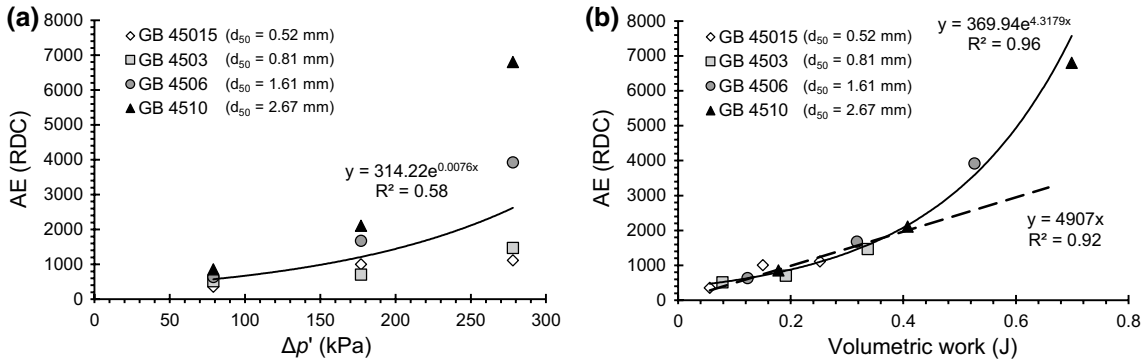

Fig. 6 Results from isotropic compression tests to effective confining pressures of 100, 200 and 300 kPa performed on glass beads (Tests 1–9 and 12–14). **a** Total generated AE (RDC) versus change in mean effective stress (kPa). **b** Total generated AE (RDC) versus volumetric work done (Joules)

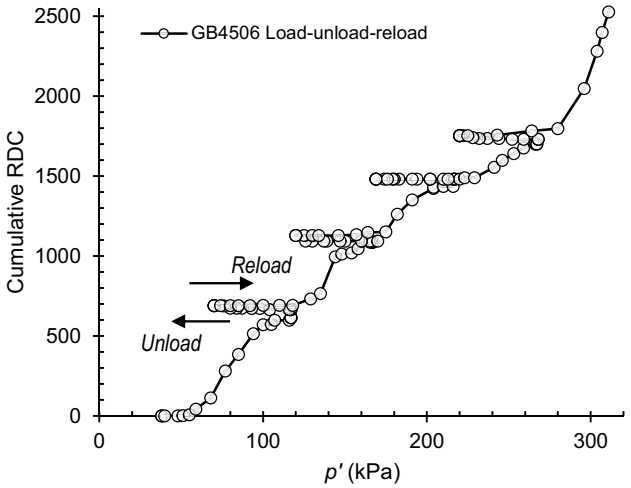

Fig. 7 Cumulative (AE) RDC versus mean effective stress (kPa) measurements for isotropic load-unload-reload cycles of cell pressure performed on GB 4506 (d_{50} = 1.61 mm) (Test 15)

greater than 0.5 J (i.e. those causing the exponential trend), shows that, in general, approximately 4900 RDC were generated per 1 Joule of volumetric work done on the glass beads. The exponential function in Fig. 6b best describes the data because both mean effective stress and density increase during isotropic compression, having a combined effect on AE generation (as described in Smith and Dixon [4]).

Figure 7 shows results from load–unload–reload cycles of cell pressure performed on GB 4506 (d_{50} = 1.61 mm) (Test 15), which demonstrates that the Kaiser Effect [38] occurs in glass beads under cycles of isotropic compression (i.e. AE activity is negligible until the current stress conditions exceed the maximum that has been experienced in the past). Imposed unload and reload stages of isotropic compression were 50 kPa and 100 kPa, respectively.

3.2 Shearing

Figure 8 shows measurements versus shear strain from GB 45015 (d_{50} = 0.52 mm) (left, Tests 1–3) and GB 4510 (d_{50} = 2.67 mm) (right, Tests 12–14). Note the periodic cycling of deviator stress, which rapidly drops and then increases as shear strength is mobilised; these cycles in deviator stress are caused by stick–slip behaviour.

AE is generated in shear by particle-scale interactions and evolving mechanisms such as inter-particle friction, stick–slip events and particle rearrangement, and hence the AE measurements have a variable nature. Mean AE rate values are presented in Fig. 8c and d for when post-peak shear strength conditions were established, which demonstrate that AE activity increased with both particle size and confining stress level: mean post-peak AE rates for GB 4510 (d_{50} = 2.67 mm) were greater than those for GB 45015 (d_{50} = 0.52 mm) by factors of 6.4, 6.1 and 5.5 for effective confining stress of 100, 200 and 300 kPa, respectively; and an increase in effective confining stress of 100 kPa (i.e. from 100 to 200 kPa and from 200 to 300 kPa) caused the mean post-peak AE rates to increase by a factor of approximately 1.4.

Figure 8 shows that the amplitude of deviator stress cycles during stick–slip events increased with confining stress level and were significantly greater for GB 45015 (d_{50} = 0.52 mm) than for GB 4510 (d_{50} = 2.67 mm) (i.e. inversely proportional to particle size). The amplitudes of deviator stress cycles were greater in the GB 45015 (d_{50} = 0.52 mm) because its shear strength was controlled by failure along a concentrated shear zone, whereas GB 4510 (d_{50} = 2.67 mm) experienced a greater distribution of shear strains and hence particle dislocations as it failed by bulging.

The stick–slip events caused cycles in AE activity and hence were the principal cause for the variable nature in AE rate measurements. The coefficient of variation (CoV) (i.e. the ratio of standard deviation to the mean) of AE rate

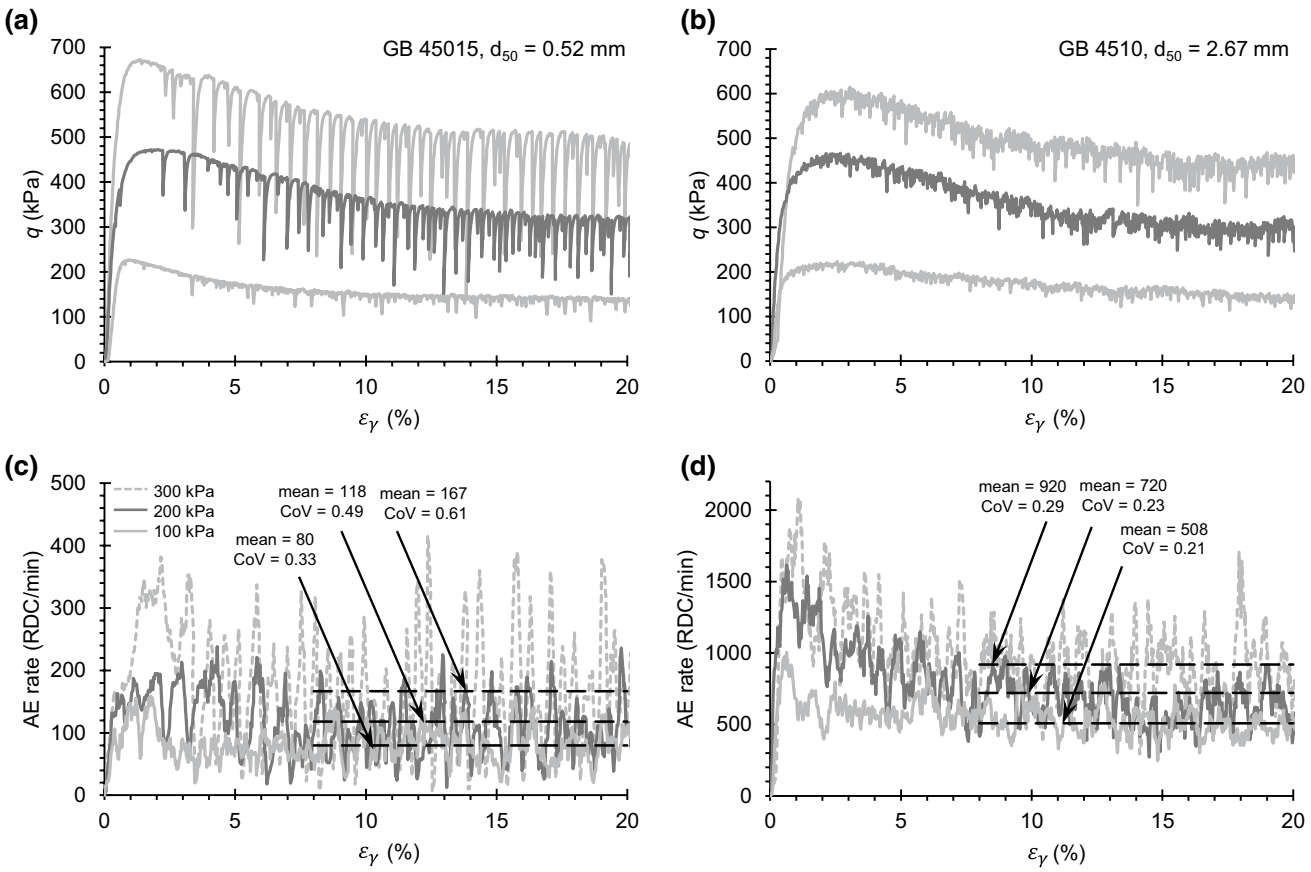

Fig. 8 Measurements versus shear strain (%) from drained triaxial shearing tests performed on GB 45015 (d_{50} = 0.52 mm) (left) and GB 4510 (d_{50} = 2.67 mm) (right) at effective confining pressures of 100, 200 and 300 kPa and axial displacement rate of 1 mm/h (Tests 1–3 and 12–14). **a**, **b** deviator stress (kPa), and **c**, **d** AE rate (RDC/min)

measurements during post-peak conditions was calculated as a measure of this variability and the calculated CoV values for GB 45015 (d_{50} = 0.52 mm) and GB 4510 (d_{50} = 2.67 mm) are presented in Fig. 8c and d, respectively. The calculated CoV values for GB 45015 (d_{50} = 0.52 mm) were greater than those for GB 4510 (d_{50} = 2.67 mm) by factors of 1.6, 2.1 and 2.1 for effective confining stress of 100, 200 and 300 kPa, respectively. In addition, an increase in effective confining stress caused the calculated CoV values to increase by factors of 1.5 (from 100 to 200 kPa) and 1.2 (from 200 to 300 kPa) for GB 45015 (d_{50} = 0.52 mm), and by factors of 1.1 (from 100 to 200 kPa) and 1.3 (from 200 to 300 kPa) for GB 4510 (d_{50} = 2.67 mm).

Figure 9 shows measurements versus shear strain from Tests 9, 10 and 11 (GB 4506; d_{50} = 1.61 mm) to demonstrate the influence of axial displacement rate. AE rates increased proportionally with the imposed displacement rate as more particle-scale interactions took place per unit time. AE generation increased with shear strain and reached peak values that were maintained from volume minimum (i.e. the transition from contractive to dilative behaviour) to peak dilatancy, whereupon AE generation gradually reduced and then remained around a constant mean value with further increments of shear strain. Average AE rates measured during post-peak shear strength behaviour are plotted against the applied axial displacement rate in Fig. 10, which results in a linear relationship with strong correlation (R^2 of 0.99) over the range of data examined. Note that Smith and Dixon [39] observed a non-linear AE rate versus displacement rate relationship for granular media (i.e. a power curve intersecting the origin); therefore, the power curve plotted in Fig. 10 (R^2 of 0.99) more accurately extrapolates the AE response at slower displacement rates.

Figure 11 shows calculated work done (boundary, distortional and volumetric) versus shear strain during all tests performed on GB 4506 (d_{50} = 1.61 mm) (Tests 7–11) (i.e. under different imposed effective confining stresses and axial displacement rates), which shows that work done was governed by stress level but independent of axial displacement rate, as would be expected for the range of strain rates applied (i.e. negligible strain rate effects were

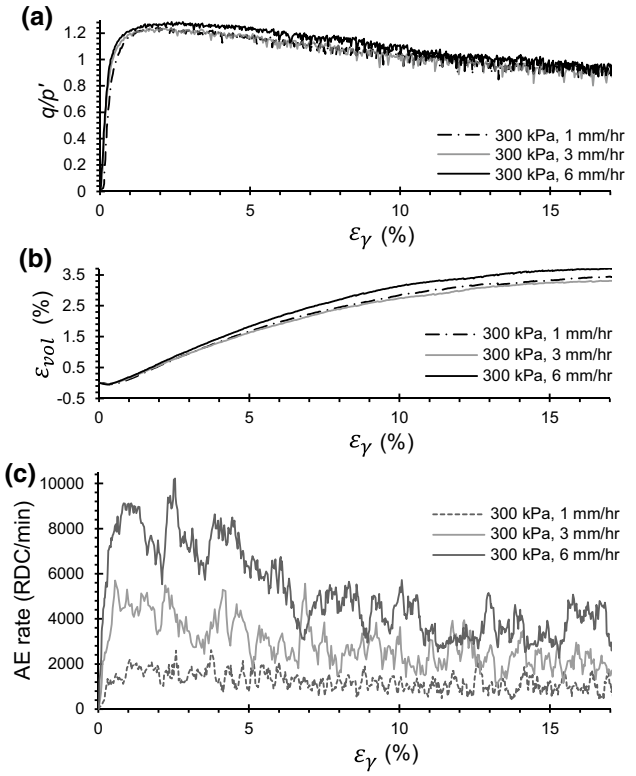

Fig. 9 Measurements versus shear strain (%) from drained triaxial shearing tests performed on GB 4506 (d_{50} = 1.61 mm) at an effective confining pressure of 300 kPa and axial displacement rates of 1, 3 and 6 mm/h (Tests 9–11). **a** Stress ratio (q/p′), **b** volumetric strain (%) (dilation shown as positive), and **c** AE rate (RDC/min)

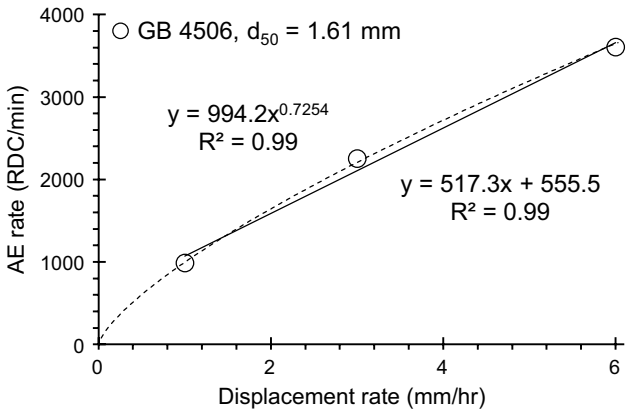

Fig. 10 AE rate (RDC/min) versus displacement rate (mm/h) relationship (linear and power regressions) obtained from drained triaxial shearing tests at an effective confining pressure of 300 kPa and axial displacement rates of 1, 3 and 6 mm/h for GB 4506 (d_{50} = 1.61 mm) (Tests 9–11). The AE rate (RDC/min) values shown are averages calculated after mobilisation of peak shear strength (i.e. post-peak)

observed). The average AE rate versus boundary work rate relationships for Tests 1–14 are compared in Fig. 12 during peak (i.e. volume minimum to peak dilatancy) and

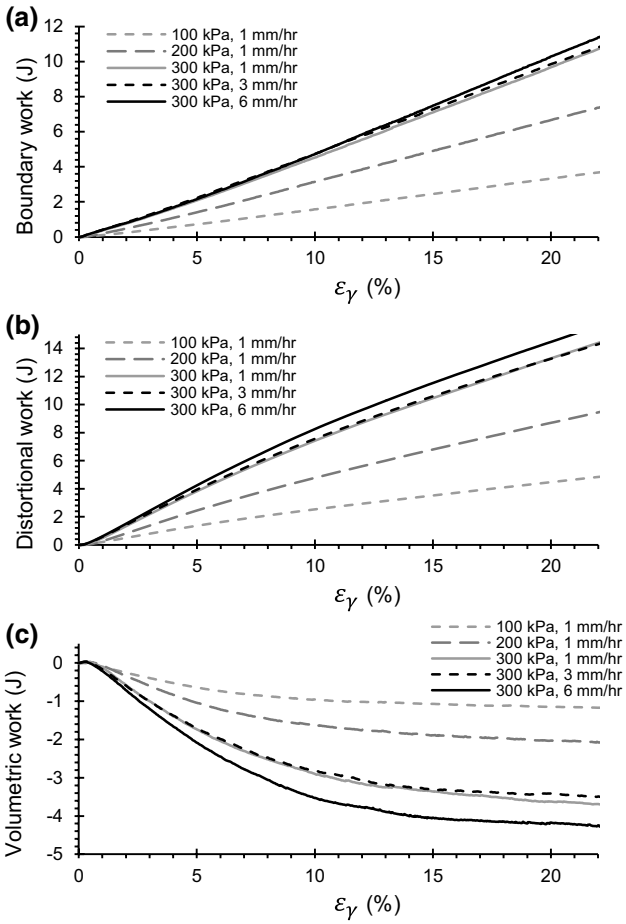

Fig. 11 Measurements from drained triaxial shearing tests performed on GB 4506 (d_{50} = 1.61 mm) (Tests 7–11). **a** boundary work (J) versus shear strain (%), **b** distortional work (J) versus shear strain (%), and **c** volumetric work (J) versus shear strain

post-peak conditions. Linear regressions with R^2 values of 0.95 and 0.90 were obtained during peak and post-peak conditions, respectively. The gradient of the relationship (i.e. AE generated per Joule) representing peak conditions in shear is 1.8 times greater than the relationship representing post-peak conditions. Moreover, when Fig. 12 is compared with Fig. 5, it can be concluded that glass beads generate between 18 (peak) and 10 (post-peak) times greater AE per Joule of work in shear than they do in isotropic compression.

Figure 13 shows measurements of stress ratio, volumetric strain and AE rates up to 5% of axial strain during Test 3 (GB 45015, d_{50} = 0.52 mm, 300 kPa, 1 mm/h), which exemplify the observed AE rate behaviour during stick–slip events. In each stick–slip event, AE activity increased during shear strength mobilisation (i.e. during the periods in Fig. 13b when the stress ratio, *q/p′*, was increasing), particle climbing and dilation (i.e. the particles override at points of contact causing the volume to increase, which occurs in

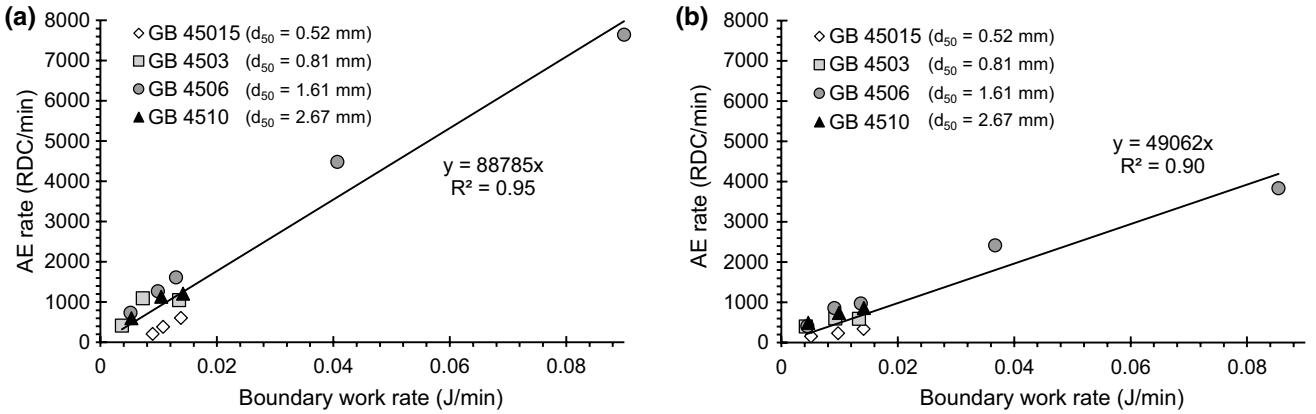

Fig. 12 Average AE rate (RDC/min) measurements versus average boundary work rate (J/min) measurements (Tests 1–14) at: **a** peak, and **b** post-peak

densely packed assemblages of particles in shearing), and then reduced with the subsequent deviator stress drop during particle sliding and contraction. Figure 14 shows the magnitude of AE rate change plotted against the amplitude of deviator stress cycles for all stick–slip events measured during Tests 1 to 3 (GB 45015, $d_{50}=0.52$ mm), which results in a linear regression with R^2 of 0.77.

Figure 15a focuses on a stick–slip event that took place between 1.8 and 2.1% of axial strain in Test 3 (GB 45015, $d_{50}=0.52$ mm, 300 kPa) (i.e. the same test as that presented in Fig. 13), which exemplifies the observed *b-value* behaviour during stick–slip events. During the stress release phase (i.e. deviator stress drop), *b-values* increased due to the AE waveform being dominated by low amplitude events. As shear strength was mobilised (i.e. when the stress ratio, *q/p'*, was increasing), *b-values* reduced as the measured AE waveform became increasingly dominated by higher amplitude events.

Figure 15b illustrates how the AE amplitude-frequency spectra changed during stick–slip events: the grey line shows the AE amplitude-frequency spectra at 1.88% axial strain (i.e. when the stress ratio was minimum in Fig. 15a), and the black line shows the AE amplitude-frequency spectra at 2.02% axial strain (i.e. during shear strength mobilisation). Above frequencies greater than approximately 11.5 kHz, significantly greater AE energy was generated during the shear strength mobilisation phase than in the stress release phase of the stick–slip event. Below frequencies of approximately 11.5 kHz, greater AE energy was generated during stress release (insert in Fig. 15b). The AE measurement system filtered frequencies below 10 kHz; however, previous studies have demonstrated high levels of AE at frequencies below 10 kHz during the stress release phase of stick–slip events (e.g. [7, 19, 21]). Note that the resonant frequency of the transducer was 30 kHz, which was the cause of the peak in AE response around this frequency.

Figure 16 compares the AE rate measurements obtained from Tests 1–14. AE rate measurements during peak conditions were greater than those during post-peak conditions in each test, evidenced by the negative AE rate difference between peak and post-peak conditions in Fig. 16a. The general trends of AE activity increasing with confining stress level, particle size and axial displacement rate are also evident in Fig. 16a. Figure 16b shows that the variability in AE rate measurements (i.e. CoV) due to stick–slip behaviour increased with confining stress level but reduced with particle size (i.e. the amplitude of AE activity cycles during stick–slip were inversely proportional to particle size). The most significant differences in CoV trends are between GB 45015 ($d_{50}=0.52$ mm) and the other three particle sizes: GB 45015 ($d_{50}=0.52$ mm) failed along a concentrated shear zone while GB 4503 ($d_{50}=0.81$ mm), GB 4506 ($d_{50}=1.61$ mm) and GB 4510 ($d_{50}=2.67$ mm) all failed by bulging.

4 Discussion

A programme of drained triaxial tests have been performed on densely packed glass beads to establish quantified relationships for use in the interpretation of mechanical behaviour from AE measurements. The mechanical behaviour of the glass beads was consistent with findings reported in the literature: the obtained critical state friction angles of 23° and dilatancy components ($\phi'_p - \phi'_{cv}$, Table 2) of 8° are typical for densely packed glass beads (e.g. [31]).

The original contributions from this study include: (i) the combination of AE rate and *b-values* has been measured from densely packed assemblages of glass beads for the first time in triaxial isotropic compression and shearing; (ii) the results show that AE generation in densely packed

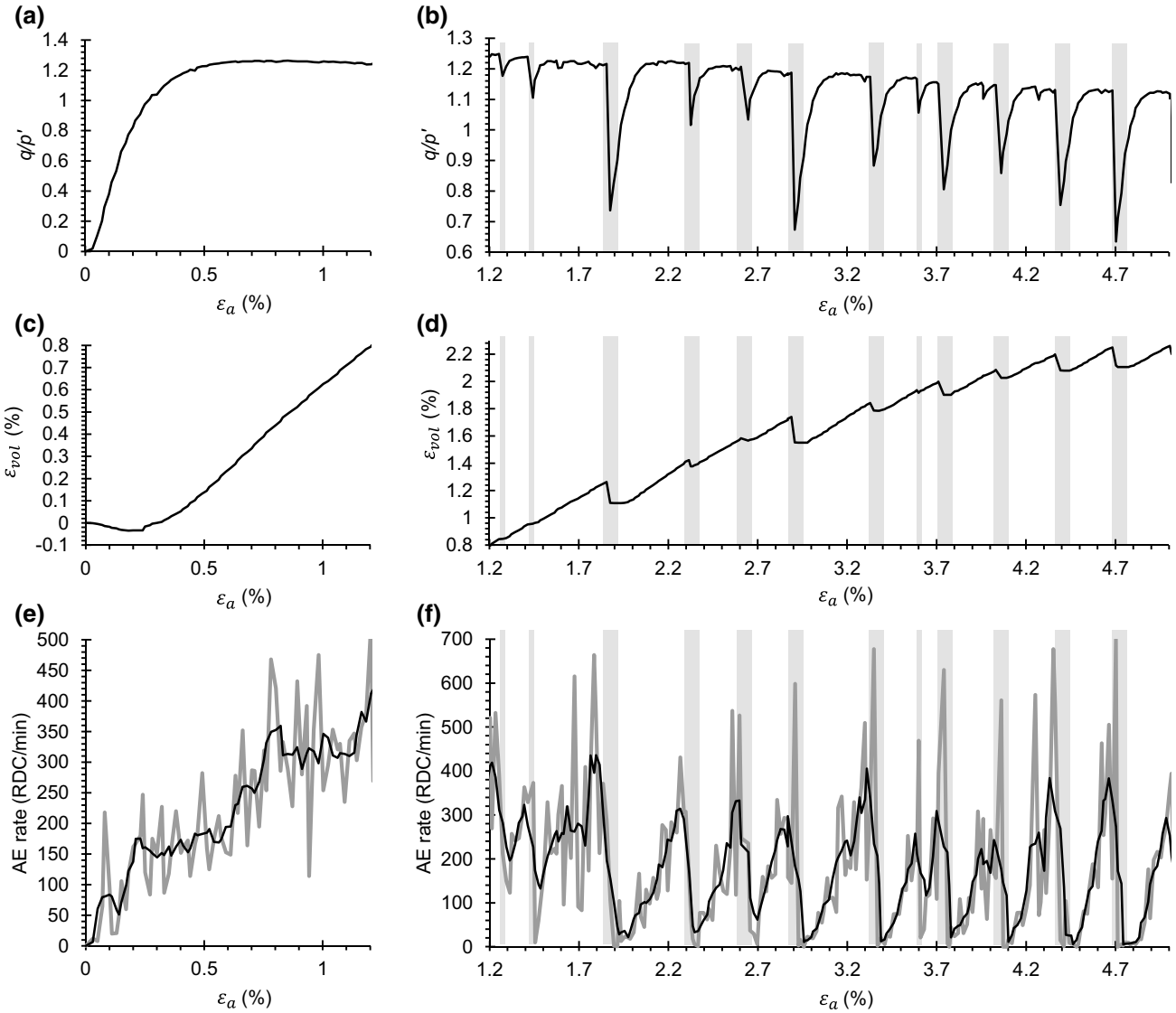

Fig. 13 Measurements versus axial strain (%) from a drained triaxial shearing test performed on GB 45015 (d_{50} = 0.52 mm) at an effective confining pressure of 300 kPa and axial displacement rate of 1 mm/h (Test 3). **a** stress ratio (q/p′) from 0 to 1.2% axial strain, **b** stress ratio (q/p′) from 1.2 to 5.0% axial strain, **c** volumetric strain (%) (dilation shown as positive) from 0 to 1.2% axial strain, **d** volumetric strain (%) (dilation shown as positive) from 1.2 to 5.0% axial strain, **e** AE rate (RDC/min) from 0 to 1.2% axial strain, and **f** AE rate (RDC/min) from 1.2 to 5.0% axial strain. The black line in **e** and **f** shows moving averages of AE rates. The vertical grey boxes in **b**, **d** and **f** highlight the timing of deviator stress drops

glass beads is proportional to the imposed stress level and displacement rate (e.g. an AE rate versus imposed displacement rate relationship has been quantified with an R^2 value of 0.99); (iii) previous research has demonstrated that natural soils experience the Kaiser Effect (e.g. [1, 4]) and this study has extended knowledge to demonstrate its existence in densely packed glass beads (i.e. AE activity is negligible until the current stress conditions exceed the maximum that has been experienced in the past); (iv) relationships have been quantified between AE and boundary work (i.e. AE generated per Joule) for a unit volume of glass beads under isotropic compression and shear (R^2 values ranging from 0.90 to 0.96), which show that glass beads generate greater RDC/J in shear than they do in isotropic compression (e.g. approximately 4900 RDC/J in isotropic compression, 49,000–89,000 RDC/J in shear) and the glass beads generated greater RDC/J in shear during peak conditions (approximately 89,000) than during post-peak conditions (approximately 49,000) because the specimens dilated and had a higher void ratio during post-peak conditions; and (v) the relationship between the amplitudes of cycles in

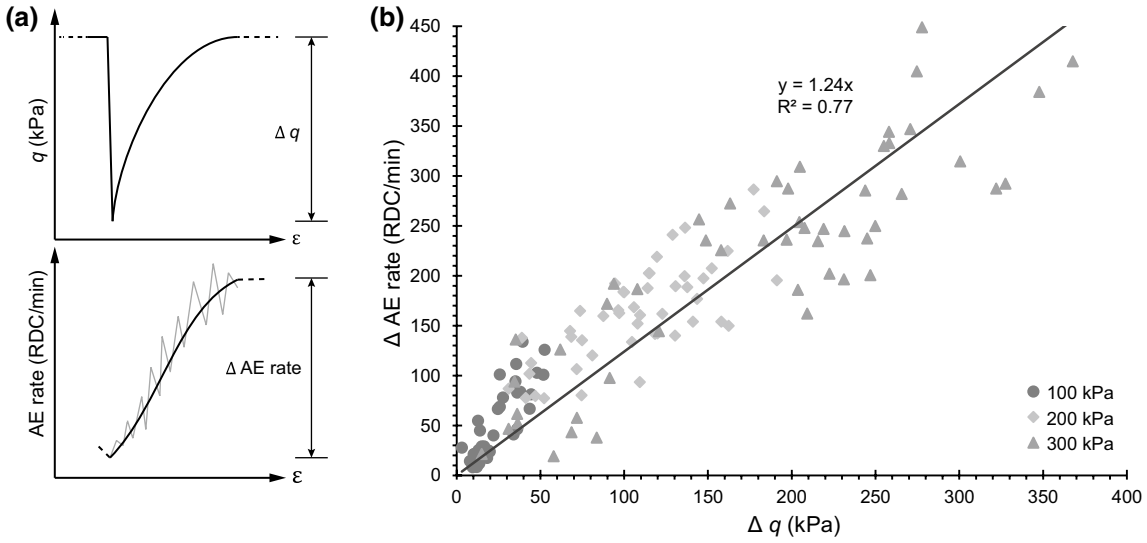

Fig. 14 **a** Illustration of changes in deviator stress and AE rates during stick–slip events. **b** ΔAE rate (RDC/min) versus Δq (kPa) relationship for all stick–slip events measured from GB 45015 (d_{50} = 0.52 mm) (Tests 1–3)

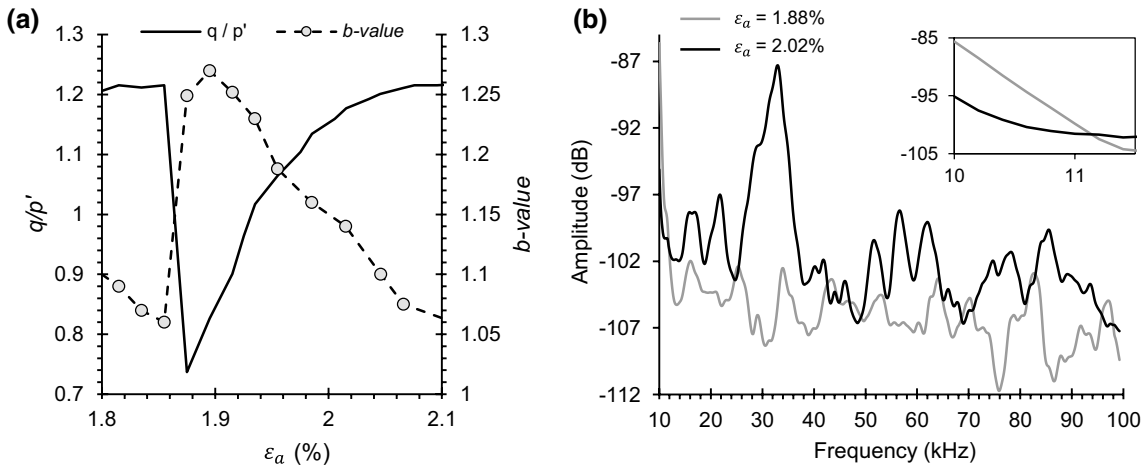

Fig. 15 Measurements from a drained triaxial shearing test performed on GB 45015 (d_{50} = 0.52 mm) at an effective confining pressure of 300 kPa and axial displacement rate of 1 mm/h (Test 3): **a** stress ratio and *b-value* versus axial strain, and **b** AE amplitude-frequency spectra at axial strains of 1.88% and 2.02% (the insert focuses on the AE amplitude-frequency spectra between 10.0 and 11.5 kHz)

deviator stress and AE activity during stick–slip events has been quantified (e.g. 1.24 RDC/min per kPa).

These findings mean that the AE interpretation framework proposed by Smith and Dixon [4] for natural sands can be extended to include densely packed glass beads and used to identify the transition from contractive to dilative behaviour (i.e. q/p' = M), mobilisation of peak shear strength and quantify accelerating deformation behaviour that typically accompanies shear zone development. The influence of fabric (e.g. density and grading) was excluded as a variable from this investigation by focusing on four poorly-graded, single-sized glass beads; however, Smith and Dixon [4] demonstrated that AE generation increases with fabric coordination number (i.e. the number of particle contacts per particle). In addition, all four glass beads had comparable shape and roughness properties, and hence these were also excluded as variables from the investigation. However, it should be noted that the glass beads were not perfectly smooth spheres (e.g. Fig. 3) and their particle shape and surface features would have influenced inter-particle friction and hence AE generation.

The study results show that stick–slip behaviour significantly influenced the AE generated by densely packed glass beads in shear: in each stick–slip event, AE activity increased (i.e. AE rates increased, and *b-values* reduced) during shear strength mobilisation, particle climbing and dilation, and

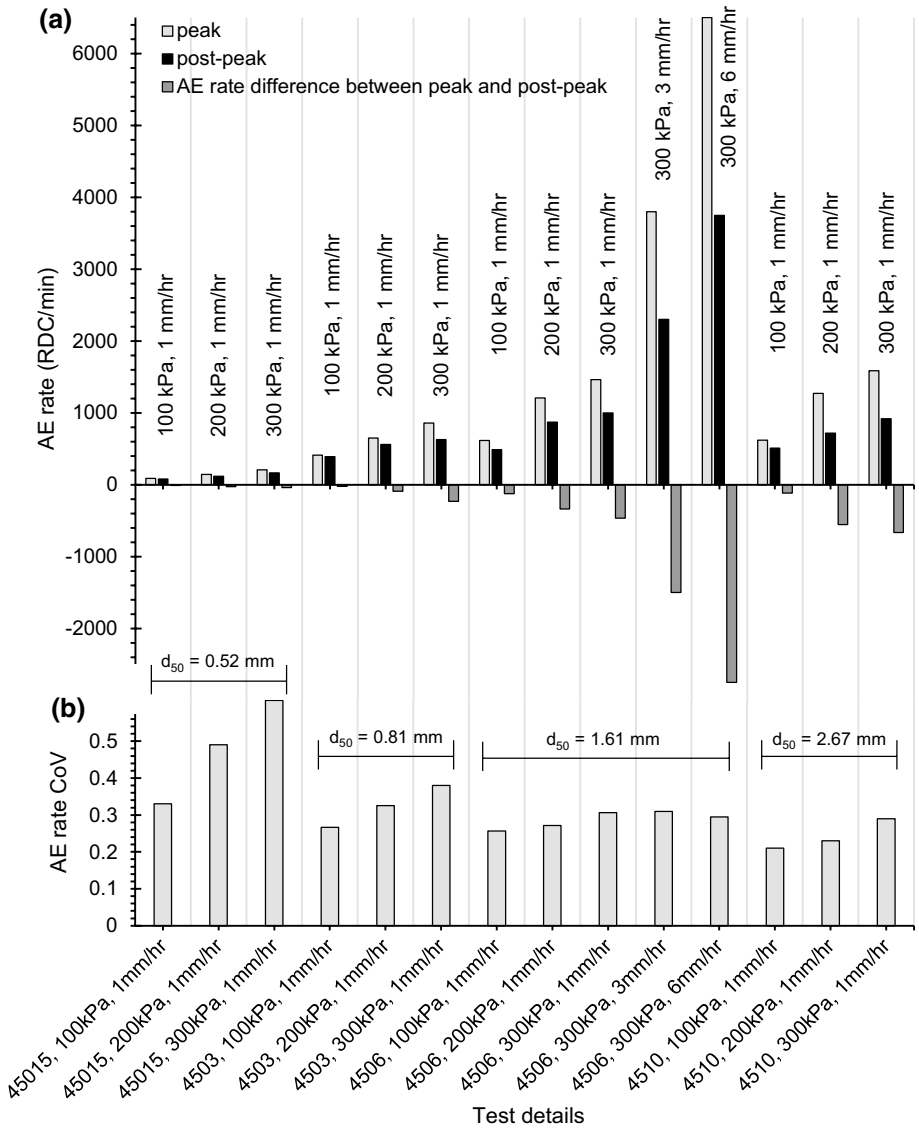

Fig. 16 Summary of measurements obtained from drained triaxial shearing tests performed on glass beads (Tests 1–14). **a** average AE rate (RDC/min) measured at peak and post-peak, and the AE rate difference between peak and post-peak; **b** coefficient of variation (CoV) of AE rate (RDC/min) measurements during post-peak behaviour

then reduced with the subsequent deviator stress drop during particle sliding and contraction. The results also show that above frequencies greater than approximately 11.5 kHz, significantly greater AE energy was generated during the shear strength mobilisation phase than in the stress release phase of stick–slip events, whereas below frequencies of approximately 11.5 kHz, greater AE energy was generated during stress release, which agrees with previous findings.

For example, Michlmayr et al. [12] and Michlmayr and Or [19] performed direct-shear experiments on glass beads using two AE measurement systems, one constrained to within 0–20 kHz (i.e. low-frequency) and one constrained to within 30–80 kHz (i.e. high-frequency). They found that AE activity was more significant in the low-frequency system during the stress release phase of stick–slip events, and in the high-frequency system during shear strength mobilisation and dilation. Johnson et al. [20] subjected layers of glass beads to granular shearing and monitored AE within 34–45 kHz; they observed significant AE activity during shear strength mobilisation and dilation. These relatively high-frequency monitoring systems (i.e. 30–80 kHz and 34–45 kHz) fall within the frequency range used in this study of 10–100 kHz, which strengthens the evidence to conclude that AE generated during the stress release phase of stick–slip events is predominantly low frequency (< 20 kHz), and AE generated during shear strength mobilisation and dilation is predominantly high frequency (> 20 kHz). Uniquely, the influence of stick–slip behaviour in densely packed glass beads on AE generation has been quantified in this study through a series of relationships (e.g. Figs. 13, 14, 15 and 16).

The implications of the findings have primarily been discussed within the context of soil mechanics with applications for geotechnical engineering and the potential to detect

changes in behaviour for use in early warning of serviceability and ultimate limit state failures. However, the newly developed quantified interpretation of AE generated by glass beads has implications for a wide range of disciplines, for example: faulting and earthquakes, granular physics, additive manufacturing, mining and pharmaceuticals.

This study has quantified links between particulate materials' physical properties, imposed conditions (i.e. stress and strain) and generated AE. The authors acknowledge, however, that in many applications, such as with natural soils, the physical properties will be highly variable and largely unknown, which would make quantitative interpretation more difficult. Smith et al. [6] demonstrated that a generic AE rate versus displacement rate relationship can be obtained for a range of granular materials (e.g. sands and gravels with a range of angularities and particle size distributions), which means, for example, that AE monitoring could be used to quantify accelerating deformation behaviour in particulate systems with only a limited knowledge of their physical properties.

5 Conclusions

This study has gone beyond the state-of-the-art and established quantitative interpretation of AE generated by densely packed glass beads in isotropic compression and shear. This new knowledge will enable the evolution of particulate material behaviour to be interpreted from AE measurements, potentially removing or reducing the need for arduous measurements of stresses and strains, and hence benefitting a wide range of applications and industries. Results from a programme of drained triaxial tests on densely packed glass beads show that:

- AE generation in densely packed glass beads is influenced by the imposed stress level, imposed displacement rate, mean particle size, the boundary work done and volumetric strain (i.e. dilation increases the void ratio and reduces the number of particle contacts per particle, and hence reduces AE activity);
- AE activity in glass beads is negligible until the current stress conditions exceed the maximum that has been experienced in the past due to the Kaiser Effect;
- Relationships between AE and boundary work (i.e. RDC generated per Joule) have been quantified for a unit volume of glass beads under isotropic compression and shear, which show that significantly greater RDC/J is generated in shear than in isotropic compression;
- An AE rate versus displacement rate relationship has been quantified, which enables interpretation of accelerating deformation behaviour that typically accompanies shear zone development following mobilisation of peak shear strength in dense particulate materials;
- Stick–slip behaviour significantly influenced AE generation in shear: in each stick–slip event, AE activity increased during shear strength mobilisation, particle climbing and dilation, and then reduced with the subsequent deviator stress drop during particle sliding and contraction. The amplitude of these cycles in AE activity were proportional to the amplitude of deviator stress cycles during stick–slip events, which were also proportional to the imposed stress level and inversely proportional to particle size.

Acknowledgements The authors acknowledge the excellent technical assistance provided by Mr Lewis Darwin and the Loughborough Materials Characterisation Centre. Alister Smith gratefully acknowledges the support of an EPSRC Fellowship (Listening to Infrastructure, EP/P012493/1). Data reported in this study can be made available by the authors on request.

Compliance with ethical standards

Conflict of interest The authors declare that they have no conflict of interest.

References

1. Koerner, R.M., McCabe, W.M., Lord, A.E.: Acoustic Emission Behavior and Monitoring of Soils. In: Drnevich, V.P., Gray, R.E. (eds.) Acoustic emissions in geotechnical engineering practice ASTM STP 750, pp. 93–141. ASTM International, West Conshohocken (1981)
2. Tanimoto, K., Tanaka, Y.: Yielding of soil as determined by acoustic emission. Soils Found. **26**(3), 69–80 (1986)
3. Naderi-Boldaji, M., Bahrami, M., Keller, T., Or, D.: Characteristics of acoustic emissions from soil subjected to confined uniaxial compression. Vadose Zone J., **16**(7), 1–12 (2017)
4. Smith, A., Dixon, N.: Acoustic emission behaviour of dense sands. Géotechnique https://doi.org/10.1680/jgeot.18.P.209 (2019)
5. Smith, A., Dixon, N., Meldrum, P., Haslam, E., Chambers, J.: Acoustic emission monitoring of a soil slope: Comparisons with continuous deformation measurements. Géotech Lett **4**(4), 255–261 (2014)
6. Smith, A., Dixon, N., Fowmes, G.: Early detection of first-time slope failures using acoustic emission measurements: large-scale physical modelling. Géotechnique **67**(2), 138–152 (2017)
7. Michlmayr, G., Chalari, A., Clarke, A., Or, D.: Fiber-optic high-resolution acoustic emission (AE) monitoring of slope failure. Landslides **14**(3), 1139–1146 (2017)
8. Dixon, N., Smith, A., Flint, J. A., Khanna, R., Clark, B., Andjelkovic, M.: An acoustic emission landslide early warning system for

communities in low-income and middle-income countries. Landslides https://doi.org/10.1007/s10346-018-0977-1 (2018)
9. Adjemian, F., Evesque, P.: Experimental study of stick-slip behaviour. Int. J. Numer. Anal Methods Geomech. **28**(6), 501–530 (2004)
10. Johnson, P.A., Savage, H., Knuth, M., Gomberg, J., Marone, C.: Effects of acoustic waves on stick–slip in granular media and implications for earthquakes. Nature **451**(7174), 57 (2008)
11. Bonneau, L., Catelin-Jullien, T., Andreotti, B.: Friction-induced amplification of acoustic waves in a low Mach number granular flow. Phys. Rev. E **82**(1), 011309 (2010)
12. Michlmayr, G., Cohen, D., Or, D.: Shear-induced force fluctuations and acoustic emissions in granular material. J. Geophys. Res. Solid Earth **118**(12), 6086–6098 (2013)
13. McNamara, S.C.: Acoustics and frictional sliding in granular materials. Granul. Matter **17**(3), 311–324 (2015)
14. Everton, S.K., Hirsch, M., Stravroulakis, P., Leach, R.K., Clare, A.T.: Review of in situ process monitoring and in situ metrology for metal additive manufacturing. Mater. Des. **95**, 431–445 (2016)
15. Li, J., Huang, Y., Chen, Z., Li, M., Qiao, M., Kizil, M.: Particle-crushing characteristics and acoustic-emission patterns of crushing gangue backfilling material under cyclic loading. Minerals **8**(6), 244 (2018)
16. Serris, E., Périer-Camby, L., Thomas, G., Desfontaines, M., Fantozzi, G.: Acoustic emission of pharmaceutical powders during compaction. Powder Technol. **128**(2–3), 296–299 (2002)
17. Papp, M.K., Pujara, C.P., Pinal, R.: Monitoring of high-shear granulation using acoustic emission: predicting granule properties. J. Pharm. Innov. **3**(2), 113–122 (2008)
18. Sadrekarimi, A., Olson, S.M.: Critical state friction angle of sands. Géotechnique **61**(9), 771 (2011)
19. Michlmayr, G., Or, D.: Mechanisms for acoustic emissions generation during granular shearing. Granul. Matter **16**(5), 627–640 (2014)
20. Johnson, P.A., Ferdowsi, B., Kaproth, B.M., Scuderi, M., Griffa, M., Carmeliet, J., Guyer, R.A., Le Bas, P.Y., Trugman, D.T., Marone, C.: Acoustic emission and microslip precursors to stick-slip failure in sheared granular material. Geophys. Res. Lett. **40**(21), 5627–5631 (2013)
21. Cui, D., Wu, W., Xiang, W., Doanh, T., Chen, Q., Wang, S., Liu, Q., Wang, J.: Stick-slip behaviours of dry glass beads in triaxial compression. Granul. Matter **19**(1), 1 (2017)
22. Bishop, A.W., Wesley, L.D.: A hydraulic triaxial apparatus for controlled stress path testing. Géotechnique **25**(4), 657–670 (1975)
23. BS EN ISO 17892: Geotechnical investigation and testing – laboratory testing of soil. London, UK: BSI (2016)
24. Zheng, J., Hryciw, R.D.: Traditional soil particle sphericity, roundness and surface roughness by computational geometry. Géotechnique **65**(6), 494–506 (2015)
25. Krumbein, W.C., Sloss, L.L.: Stratigraphy and Sedimentation, 2nd edn. Freeman and Company, San Francisco, CA, USA (1963)
26. Cho, G.C., Dodds, J., Santamarina, J.C.: Particle shape effects on packing density, stiffness, and strength: natural and crushed sands. J. Geotech. Geoenviron. Eng. **132**(5), 591–602 (2006)
27. Cavarretta, I., Coop, M., O'Sullivan, C.: The influence of particle characteristics on the behaviour of coarse grained soils. Géotechnique **60**(6), 413–423 (2010)
28. Head, K. H.: Manual of Laboratory Testing. Volume 3: Effective Stress Tests, ELE International Ltd (1986)
29. Been, K., Jefferies, M.G., Hachey, J.: Critical state of sands. Géotechnique **41**(3), 365–381 (1991)
30. Skempton, A.W.: The pore-pressure coefficients A and B. Geotechnique **4**(4), 143–147 (1954)
31. Wu, K., Abriak, N., Becquart, F., Pizette, P., Remond, S., Liu, S.: Shear mechanical behavior of model materials samples by experimental triaxial tests: case study of 4 mm diameter glass beads. Granul. Matter. **19**(4), 65 (2017)
32. Muir Wood, D.: Soil behaviour and critical state soil mechanics. Cambridge University Press, Cambridge, UK (1990)
33. Bolton, M.D.: A Guide to Soil Mechanics. Universities Press, Oxford (2003)
34. Powrie, W.: Soil Mechanics: Concepts and Applications. CRC Press, Boca Raton (2013)
35. Hanley, K.J., Huang, X., O'Sullivan, C.: Energy dissipation in soil samples during drained triaxial shearing. Géotechnique **68**(5), 421–433 (2017)
36. Mao, W., Towhata, I.: Monitoring of single-particle fragmentation process under static loading using acoustic emission. Appl. Acoust. **94**, 39–45 (2015)
37. Pollock, A.A.: Acoustic emission-2: acoustic emission amplitudes. Non-destr. Test. **6**(5), 264–269 (1973)
38. Lavrov, A.: The Kaiser effect in rocks: principles and stress estimation techniques. Int. J. Rock Mech. Min. Sci. **40**(2), 151–171 (2003)
39. Smith, A., Dixon, N.: Quantification of landslide velocity from active waveguide-generated acoustic emission. Can. Geotech. J. **52**(4), 413–425 (2015)